

ZnO@ZIF-8: Gas sensitive core-shell hetero-structures show reduced cross-sensitivity to humidity

Sreeja Sreedharan Nair^{1,*}, Navas Illyaskutty^{2,*}, Benjamin Tam³, A. Ozgur Yazaydin³, Katja Emmerich⁴, Annett Steudel⁴, Tawheed Hashem¹, Ludger Schöttner¹, Christof Wöll¹, Heinz Kohler^{2,#}, Hartmut Gliemann^{1,§}

¹Institute of Functional Interfaces (IFG), Karlsruhe Institute of Technology (KIT), Hermann-von-Helmholtz-Platz 1, 76344 Eggenstein-Leopoldshafen, Germany

²Institute for Sensor and Information Systems (ISIS), Hochschule Karlsruhe – Technik und Wirtschaft, Moltkestr. 30, 76133 Karlsruhe, Germany

³Department of Chemical Engineering, University College London, Torrington Place, London WC1E 7JE, United Kingdom

⁴Center of Material Moisture (CMM), Karlsruhe Institute of Technology (KIT), Hermann-von-Helmholtz-Platz 1, 76344 Eggenstein-Leopoldshafen, Germany

**Both authors contributed equally*

Corresponding authors: [§hartmut.gliemann@kit.edu](mailto:hartmut.gliemann@kit.edu), [#heinz.kohler@hs-karlsruhe.de](mailto:heinz.kohler@hs-karlsruhe.de)

Abstract

A ‘lawn-like’ distribution of interconnected zinc oxide nanorods, coated with a metal-organic compound based on zeolitic imidazolate frameworks – ZIF-8 was prepared on microstructured thin-film interdigitated Pt-electrodes forming ZnO@ZIF-8 core-shell heterostructures and investigated as gas sensor material in relation to the identical, but uncovered pure ZnO-layer. This composite combines the gas sensing properties of the metal oxide ZnO with the specific properties of the metal organic framework material which result in a distinct change of the conditions of gas sensing at the ZnO/ZIF-8-interface. Herein, for the first time it is reported that as prepared ZnO@ZIF-8 composite material is an attractive choice to reduce the cross-sensitivity to water vapour (humidity) in the gas sensing response towards propene and ethene. The observed change of sensitivity in relation to uncovered ZnO is discussed to be due to (i) the specific interaction of the ZIF-8 at the interface with the ZnO taking influence on the gas reaction processes, (ii) the diffusivity of ZIF-8 for the different gas components, and (iii) the sorption behaviour of the used gases at the ZnO interface and inside the ZIF-8 material.

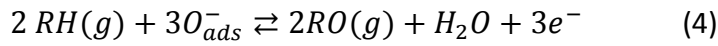
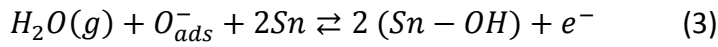
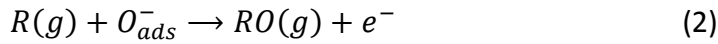
Key words

Metal oxide gas sensors, metal-organic frameworks, humidity, cross-sensitivity, ZIF-8, zink oxide

1. Introduction

Metal oxide gas (MOG) sensors are known since the mid 1950s where ZnO was used for the detection of hydrogen and other gaseous components, including CO₂, propane, ethanol, benzene and toluene [1, 2]. Starting with these basic investigations the gas/surface interaction was understood as a catalytically driven (electro-)chemical reaction of the target gases resulting in a change of the electronic states of the semiconducting oxide material, which can be detected by conductivity measurements. According to generally accepted theories the following chemical processes take place at the oxide surfaces [3, 4]. Oxygen molecules from the air adsorb on the semiconductor surface and form an $O_{2,ads}^-$ surface state or, at higher temperatures, dissociate to two surface bound negatively charged surface oxygen species O_{ads}^- (Eq. 1). In both cases one or two electrons per oxygen molecule are trapped in surface states and resulting in a surface-near electron depletion zone where the electronic conductivity is highly reduced. Consequently, the overall conductance of the porous metal oxide layer is low. Target gaseous species R(g), like CO or hydrocarbons from the adjacent gas atmosphere may be adsorbed on the surface as well and sensitively react with the charged surface oxygen states forming an oxidized gaseous species RO, which subsequently desorbs from the oxide surface by injecting the electron(s) into the conduction band of the semiconductor (Eq. 2). This results in an increase of conductivity in the space-charge layer.

The effects of water vapour on the resistance of tin oxide layers are described in different surface reaction mechanisms [5]. One of the simpler possible ways is the direct reaction of the ionosorbed oxygen (O_{ads}^-) with the adsorbed water molecule which leads to the formation of terminal hydroxyl groups while an electron is injected into the conduction band of the semiconductor (Eq. 3) [6]. Hence, in difference to the reaction with R(g) according to eq. 2, in all reaction mechanisms with water it is assumed, that the terminal OH-groups keep adsorbed after reaction and, as a consequence, may block the reaction site for further (O_{ads}^-)-formation (eq. 1) in thermodynamic equilibrium with the local H₂O partial pressure at the interface. This means, both, the humidity in the adjacent atmosphere and the water formed as a reaction product, if processes with hydrocarbons (RH) are involved [3] (Eq. 4), enhance the conductance and give rise to general cross-sensitivity of this kind of sensors.



Since the first published papers demonstrating the application of metal oxide as sensor materials huge efforts were taken to develop metal oxide-based gas sensor devices for many fields of application. As an example, a first patent has been placed by N. Taguchi in 1970 (UK Patent 1280809), where metal oxide (MO) based interfaces heated to temperatures between 300 °C and 450 °C were used as - albeit unspecific – sensor material for detection of leaks of gases in homes. During the decades great progress in the development of semiconducting metal oxide gas sensors has been reported not only in terms of optimized sensor materials, sensitivity and selectivity [7, 8], but also with respect to the integration of the sensor materials in technical environments including different approaches for miniaturization [9], minimized heating power [10] and/or the setup of sensor arrays [11]. Considerable improvement of gas analysis capability has been shown to be possible by thermocyclic operation of those (one-chip) sensor arrays and numeric analysis of the resulting conductance-over-time profiles [12, 13]. However, in spite of this great progress, cross-sensitivity to humidity is still an unsolved problem. This motivated another approach to increase the specificity of gas sensing by developing hybrid materials, i.e. by combining classical gas-sensitive metal oxides with other materials, particularly metal-organic frameworks (MOFs) [14, 15]. MOFs are a class of nanomaterials that have recently attracted attention due to their potential interest in applications that range from catalysis [16, 17], photovoltaics [18, 19], energy storage [20-22] to gas storage [23, 24] as well as sensing [25, 26]. MOFs were introduced by O. Yaghi [27] and consist of two components – (i) inorganic metal ions or metal ion-containing subunits and (ii) organic linker molecules – which form highly porous, crystalline materials by self-assembling. The geometrical, chemical and physical properties of the linker molecules can be used to tune the properties of the MOF in terms of pore geometry (size, diameter, shape) or physical properties (polarity, magnetic, electric, optical) for certain application [28]. MOFs can either be produced as a pure bulk material or as a coating of particulate systems or substrates to form hybrid materials. Hybrid materials of the category ‘semiconductor@MOF’ [15, 29-33] use silicon dioxide or metal oxides as core material and are applied for gas storage/separation and/or gas sensing. Recently, several research reports revealed the gas sensing capability of nanostructures consisting of semiconducting metal oxide cores with a MOF shell (MO@MOF) [25-28, 32] where the MOF functions as a selective gas filter or - in the case of Co-doped MOF shells - as a catalytically active layer [31].

As already stated above, even being highly sensitive to very low concentrations of inorganic gases and volatile organic compounds (VOCs), chemo-resistive semiconducting metal oxide

gas sensors often suffer from their low specific gas discriminative capability and cross-sensitivity to other gases particularly water vapour [34]. The latter aspect is particularly relevant when the composition of combustion gases has to be analysed, where water always is one of the main combustion products (see equation 3). Extensive studies have been reported in this context to overcome those limitations [35], which deals with exploring materials by functionalization of MOs with specific metals, decoration with catalysts, doping with other metal oxides and developing composite materials [13].

Within the family of Zeolitic Imidazole frameworks (ZIFs), ZIF-8 is one of these candidates to improve molecular discrimination by covering the metal oxide gas sensing layer. It is well known for its efficient separation of molecular mixtures, high permeation fluxes, high molecular separation factors [36] and the high stability against increased temperatures up to 500 °C [37]. Several ways are published in literature, how surfaces can be coated with MOFs ranging from the direct crystallization by immersing the substrate into a solution containing both components (i. e. organic linker and the inorganic building block) or by a layer-by-layer deposition (LBL) technique, where the substrate is subsequently exposed to each component separately by a dipping, spraying or rinsing process during a defined number of deposition cycles [36, 38, 39]. As an alternative the “self-sacrificial template method” [40] has been introduced as a feasible strategy for fabricating MO@MOF core-shell heterostructures [40, 41] by immersing the MO in the solution of the linker. In this case the metal oxide itself acts not only as the substrate, which has to be coated but also as the source of metal ions by partial dissolution in suitable solvents. A MOF shell is formed by the coordinative reaction between the organic linker molecules and the metal ions released by the MO material. The challenge of this method is the control over the size and morphology of the heterostructures by a careful optimisation of the reaction conditions.

Herein, we demonstrate the successful preparation of ‘lawn-like’ interconnected ZnO@ZIF-8 core-shell nanorods directly on platinum (Pt) thin-film inter-digital electrodes (IDEs) of a specifically designed, self-heated gas sensor chip [13]. The ZnO@ZIF-8 nanorods are prepared in a three-step process by applying the sacrificial template method. The gas sensing properties of this hybrid material were tested with two model gases - propene and ethene – whereupon particular attention was focused on the influence of relative humidity (rH) on the sensitivity performance of the sensor. Furthermore, Grand Canonical Monte Carlo (GCMC) simulations were carried out taking the experimental conditions into consideration in order to explain the behaviour of ZnO@ZIF-8-based sensor towards propene and ethene at different values of rH.

2. Material and methods

2.1 Preparation of sensor elements

The sensing element consists of a sensor chip with a nanostructured sensing material which was deposited in-house. Gold or platinum thin-film interdigitated electrodes (IDEs) and a Pt-heater structure were microstructured onto the top and bottom surfaces of the alumina chips, respectively, by DC magnetron sputtering, followed by UV-lithography and plasma etching. A micro-welding technique was used to contact the test structures of the sensor and to mount the sensor chip on a TO-8 header with gold wires (diameter of 100 μm). Fig. 1a shows exemplarily an image of a bonded sensor which was used for the present study. A detailed description of the sensor fabrication process is given elsewhere.[42, 43]

2.2 Synthesis of ZnO nanorods

ZnO nanostructured gas sensitive thin films were deposited onto the afore prepared Pt-IDEs via a two-step process: First a 10-nm seed layer of ZnO (Sigma Aldrich, Germany) was deposited site-selectively onto the pre-cleaned IDEs by RF magnetron sputtering (Pfeiffer Vacuum GmbH, Germany) at 100 W for 10 minutes. As it is a non-reactive sputtering without oxygen, the seeded substrates were oxidised at 400°C for 60 minutes. Afterwards, these substrates were directly used for hydrothermal growth [44] of ZnO nanorods. For this procedure 297 mg of zinc nitrate hexahydrate ($\text{Zn}(\text{NO}_3)_2 \cdot 6\text{H}_2\text{O}$) and 70 mg of hexamethylenetetramine (HMTA, both Sigma Aldrich, Germany) were solved in 20 ml of distilled water each. Both solutions were mixed and stirred well. Then 1.2 ml of an aqueous 25 wt% NH_4OH solution was added to the mixed solution to stimulate the growth of ZnO nanorods [44]. This solution was transferred to a Teflon lined stainless steel autoclave. In the next step the IDEs with ZnO seeds were placed inside the Teflon veil, with the seeded surface facing upwards. The autoclave was closed and heated to 100 °C for 24 hours. After the hydrothermal growth, the samples were rinsed de-ionized water and finally sintered at 400 °C for 60 min to ensure the complete removal of HMTA. The procedure resulted in a dense carpet-like layer of ZnO nanopillars (Fig. 2a and 2b).

2.3 Synthesis of ZnO@ZIF- 8 Core-shell hetrostructures

ZnO@ZIF-8 core-shell heterostructures were prepared by a sacrificial template assisted method [30, 32, 45, 46]. The ZnO nanorods grown on Pt-IDEs were placed inside a Teflon-lined stainless-steel autoclave containing 16 mL of a 0.48 mM solution of 2-methyl imidazole (2-Melm, Sigma Aldrich, Germany) in a 1:4 volume mixture of H_2O /dimethylformamide (DMF). The autoclave was heated in an oven at 70 °C for 24 h. After cooling to room temperature, the samples were washed with methanol and dried at 100 °C for 2 h.

2.4 Material characterization methods

The morphological analysis of the surfaces was done by an environmental scanning electron microscopy (ESEM, Field Emission Gun (FEI) Philips XL SERIES 30 ESEM-FEG (FEI Co., Eindhoven, The Netherlands), which was operated with an acceleration voltage of 10–20 kV. For improving the electrical conductivity, all measured sample have been coated with a thin layer (3-5 nm) of gold and platinum. The composition analysis was carried out by X-ray photoelectron spectroscopy with Al K_{α} -radiation ($E_{ph} = 1486.6\text{eV}$). The measurements have been carried out at room temperature in grazing emission geometry ($\theta=70^\circ$) using electron analyser R4000 (Scienta, Sweden). X-ray diffraction (XRD) measurements in out-of-plane geometry were carried out with a Bruker D8-Advance diffractometer using Cu $K_{\alpha 1}$ radiation ($\lambda=0.154\text{ nm}$). The measurements were carried out over a 2θ range of $5-40^\circ$, with a scan step of 0.05° . The thermal stability of the samples was analysed using simultaneous thermal analysis (STA).

2.5 Gas sensing studies

An automated standard gas sensor test setup [47] was used for the characterization and comparison of the sensing layers consisting of non-coated ZnO nanopillars and ZnO nanopillars coated with ZIF-8 sensing layers in terms of the response towards propene and ethene at different concentrations in synthetic air under non-humid and humid (25%, 50% and 75% rH) conditions. The corresponding sensor chips were mounted into the sensor head, which is implemented in a sealed flow cell equipped with an inlet and an outlet for well-defined gas supply [48]. A flow-through technique was used to admix a flux of synthetic air with a flux of analyte gas for a defined period of time. Humidity was adjusted by additional admixing of a well-defined flux of water saturated synthetic air ($T=21^\circ\text{ C}$) with corresponding fluxes of analyte and dry synthetic air to adjust pre-defined compositions according to the analyte exposure sequence over time shown in Fig. 3b. All sensitivity experiments were conducted under a constant chip-temperature at 350° C . Before starting the real gas exposure experiments, the test structures were aged for one week in ambient air and for another week at constant synthetic air flow.

3. Results

3.1 Growth of ZnO@ZIF-8 core shell structures

Fig. 1a-d shows the preparation principle of ZnO@ZIF-8. The growth process of the ZIF-8 shell around the ZnO nanorods by sacrificial template approach is a two-step process (see Fig. 1e): (1) partial dissolution of Zn^{2+} ions and (2) coordination of the imidazolium anions (2-Melm $^-$) with Zn^{2+} cations to form ZIF-8 crystals [30, 32, 45, 46]. In such a process, precursor composition together with reaction conditions play a vital role in the formation of desired core-shell heterostructures with a functional MO core, covered uniformly by a MOF shell.

The Zn^{2+} ions are provided by the ZnO of the nanopillars and are tetrahedrally coordinated by four nitrogen atoms of four different 2-Melm molecules. The shown crystal structure of ZIF-8 is taken from the work of Fujie *et al.* [49].

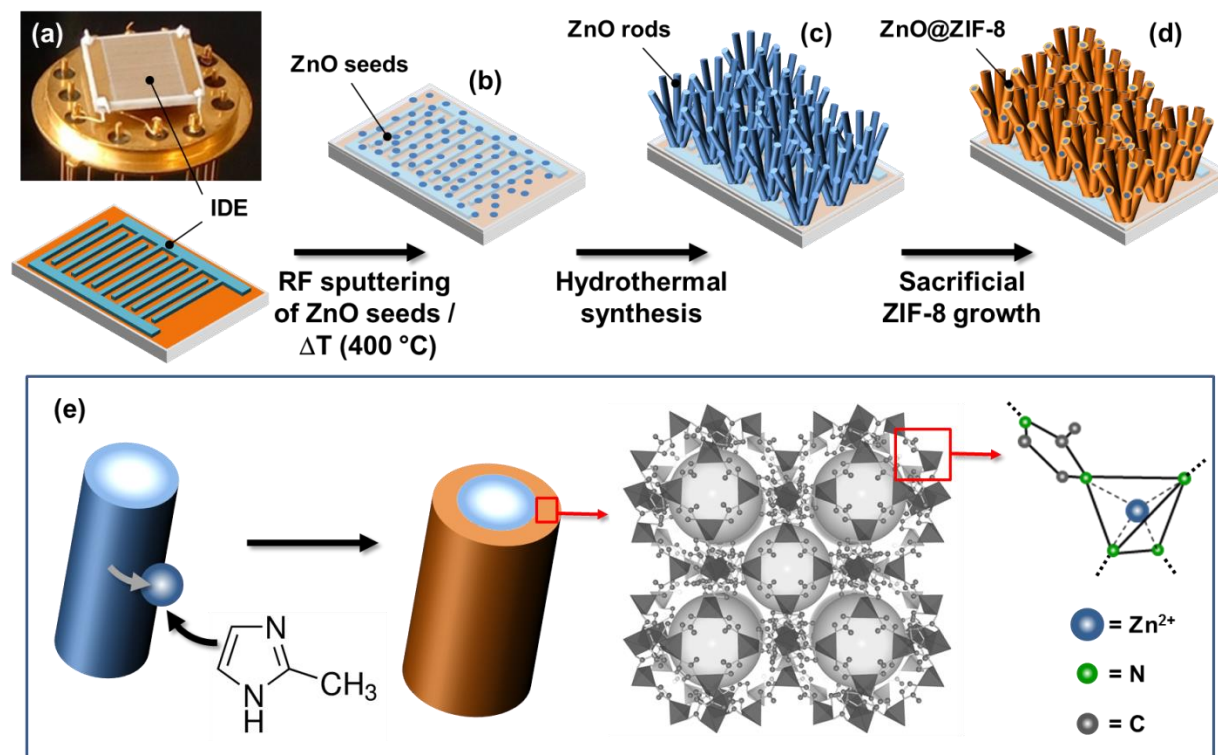


Figure 1: Schematic representation of the intermediate steps of ZnO@ZIF-8 preparation: (a) Scheme of an IDE thin-film electrode on an alumina-chip and photograph of the chip mounted in a TO8-header, (b) IDE coated with ZnO seeds after RF sputtering and temperature treatment under oxidizing conditions at 400 °C for 60 min, (c) ZnO nanopillars after hydrothermal growth, and (d) ZnO core nanopillars after sacrificial deposition of ZIF-8 shell; (e) schematic representation of the principle of sacrificial deposition of ZIF-8 shell on ZnO nanopillars. The ZIF-8 crystal structure shown in (e) is taken from the work of Fujie *et al.* [49].

The partial dissolution of ZnO nanorods to provide the Zn^{2+} ions depends on the ratio of the mixed solvents, water (H_2O)/DMF [32, 46]. Detailed investigations of the role of solvents/reaction conditions with respect to the morphology of ZIF-8 grown on ZnO have been done by several groups [30, 32, 45, 46]. Since the dissolution rate of ZnO is very fast in H_2O and slow in DMF [32], for high H_2O :DMF volume ratios, the dissolution rate of the ZnO nanorods is significantly higher than the crystallization rate of ZIF-8, which leads to an enhanced consumption of ZnO nanorods and an inhomogeneous deposition of ZIF-8 crystals along the longitudinal axis of the ZnO nanopillars. Decreasing the volume ratio H_2O :DMF retards the dissolution rate of the ZnO nanorods. Therefore, in order to avoid too fast ZnO nanorod dissolution as efficiently as possible on the one hand - which is very important for

the current work as it is the active sensing material – and to maximize the crystallization rate for ZIF-8 on the other hand, a H₂O:DMF volume ratio of 1:4 has been chosen after several trials. Besides the H₂O:DMF ratio an optimized linker (2-methyl imidazole, 2-Melm) concentration is a crucial factor for the formation of the core-shell structure and for controlling the grain size of ZIF-8 crystallites of the shell [30, 32, 45, 46]. Lower concentrations of the linker in the precursor solution result in larger ZIF-8 particles inhomogeneously deposited on the ZnO interface of the nanorods, whereas, a gradual increase of 2-Melm concentration leads to a decrease in the grain size of individual ZIF-8 crystallites resulting in a homogeneous coating of ZIF-8 around the ZnO nanorods.

It has been observed, that the growth process of ZnO@ZIF-8 starts with a heterogeneous nucleation process which takes place at the ZnO interface, followed by a diffusion-controlled growth process as soon as the interface of the ZnO is covered by the ZIF-8. The latter one is characterized by a growth which may take place on the ZnO/ZIF-8 interface as well as on the ZIF-8/linker solution interface, as both MOF components, the linker molecules and the Zn²⁺ ions, may diffuse through the pores of the ZIF-8 MOF in opposite directions [30, 32, 46].

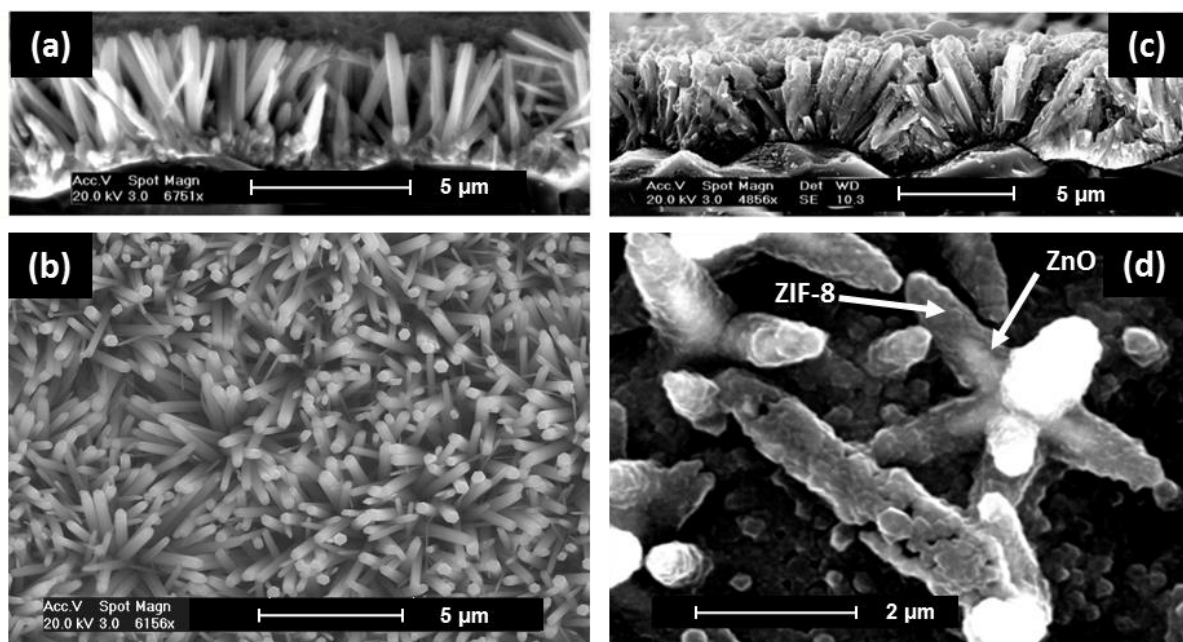


Figure 2: Scanning electron microscope images of ZnO nanopillars grown on an IDE in cross-sectional (a) and top (b) view. (c) Cross-sectional view of a ZnO@ZIF-8 core-shell structured gas sensing layer and (d) representative top view image of ZnO nanopillars coated with ZIF-8. The arrows mark the bright cone-shaped ZnO core coated by ZIF-8, depicted as a darker shell.

Surface morphology, elementary composition and thermal stability of the ZnO@ZIF-8-based gas sensor materials were analysed using XRD, XPS and STA, respectively and are presented in the Supporting Information (Figs. S1-S3). The SEM images (cross-sectional and top view) of the ZnO nanopillars and ZnO@ZIF-8 are shown in Fig. 2. Figs. 2a and b show a uniform

'lawn-like' distribution of the ZnO nanopillars forming a 3D network, inter-connecting the IDEs of the gas sensor element via inter-grown ZnO structures at the bottom forming the ZnO/IDE interface. The contact regions formed by those inter-connected nanorods enable the electrical conductivity of the sensor device and the effective resistance changes occurring by gas exposure on the ZnO interface [29]. Fig. 2(c) indicates that after the MOF deposition process the surface of the ZnO nanopillars is coated with ZIF-8. It can be observed that the initial inter-grown architecture is retained without much change in the rod dimensions apart from a coating of ZIF-8 layer. In Fig. 2d the ZnO core is shown as a bright cone which is uniformly coated by ZIF-8 which is depicted as darker shell.

3.2 Gas sensing experiments with model gases propene and ethene

Before the sensor behaviour was investigated in the presence of sample gases, the conductance of the sensor exposed with synthetic air at different rH was investigated. Fig. 3a shows the conductance of the identical sensor before (black curve) and after (red curve) the coating with ZIF-8 at 0%, 25%, 50% and 75% rH. The conductance increases with increasing humidity in both cases, whereas the effect is more pronounced for the ZnO@ZIF-8-based material.

However, the corresponding sensitivities S (see Fig. 4) which represent the relative conductance changes related to the conductance at dry air as calculated according to Eq. 5, are nearly equal for both materials, because the base line (conductance at dry air) is increased by about an order of magnitude when the ZnO nanorods are covered by ZIF-8.

$$S = \frac{G_{gas} - G_{dry\ air}}{G_{dry\ air}} \quad (5)$$

All gas sensing experiments are operated at about 350 °C at different values of rH with an analyte gas exposure sequence as shown in Fig. 3b. The gas sensing responses of the pure ZnO and the ZnO@ZIF-8 gas sensor towards propene and ethene under non-humid and humid conditions are shown in Figs. 3c and 3d. The horizontal dotted lines show that the sensor conductance one hour after the exposure to the humidified target gases (rH = 25%, 50% at 250 ppm) shows equal values compared to the case, when the target gas (250 ppm) was applied to the sensor in a first step and then humidity was increased to 25%, 50% and 75% in a second step. This confirms the high reproducibility of the conductance data even at different histories of gas exposure conditions. Fig. 4 summarizes the differences in sensitivities (Eq. 5) based on the data shown in Figs. 3a, 3c and 3d.

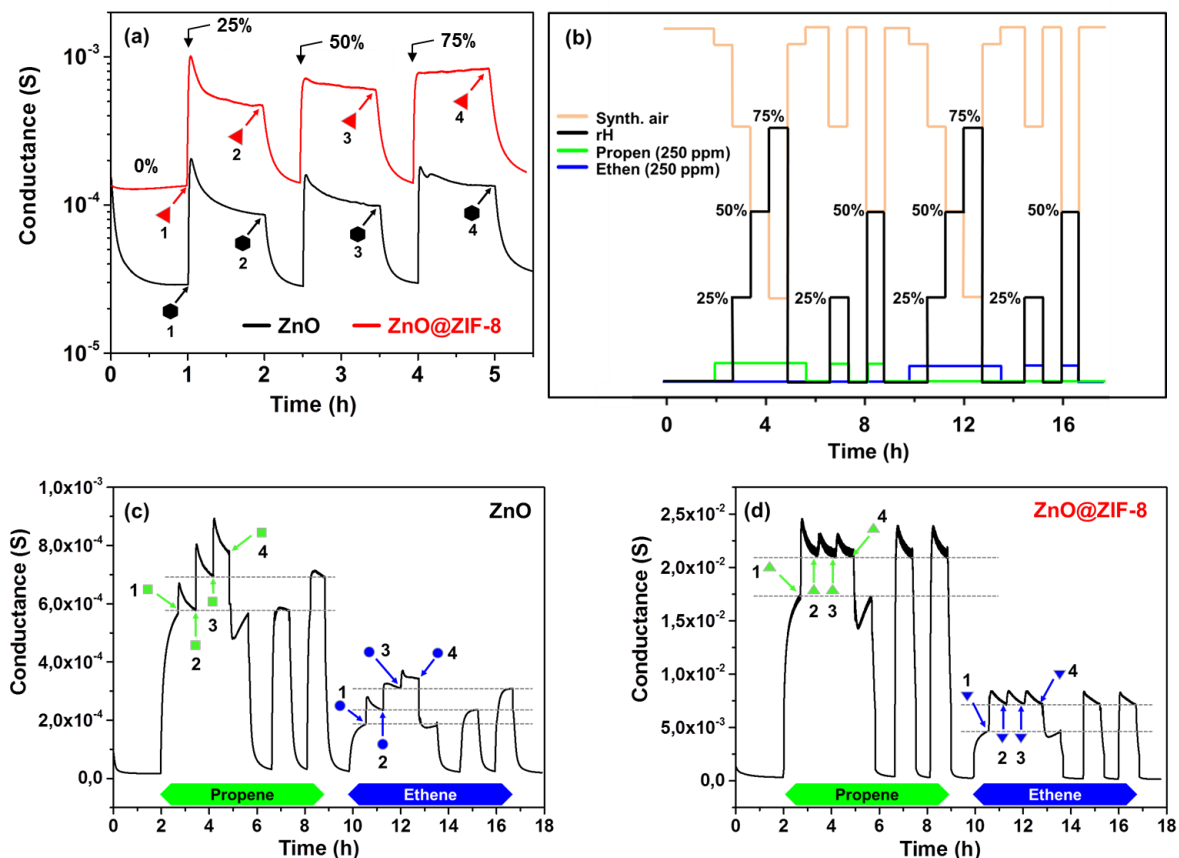


Figure 3: Conductance behaviour of a ZnO-based sensor before (black) and after (red) coating with ZIF-8. (a) Exposure of synthetic air at different rH values (0%, 25%, 50% and 75%) (b) Procedure of target gas (propene, ethene, 250 ppm each in synthetic air) exposures at different rH, adjusted by the admixture of water vapour saturated synthetic air ($T=21^{\circ}\text{C}$). Sensing responses of a ZnO-based sensor (c) before and (d) after coating with ZIF-8, respectively, according to the gas exposure procedure as shown in (b). The arrows labeled with coloured symbols and numbers mark those data points for which the sensitivities are calculated according to Eq. 5 and plotted as function of rH in Fig. 4.

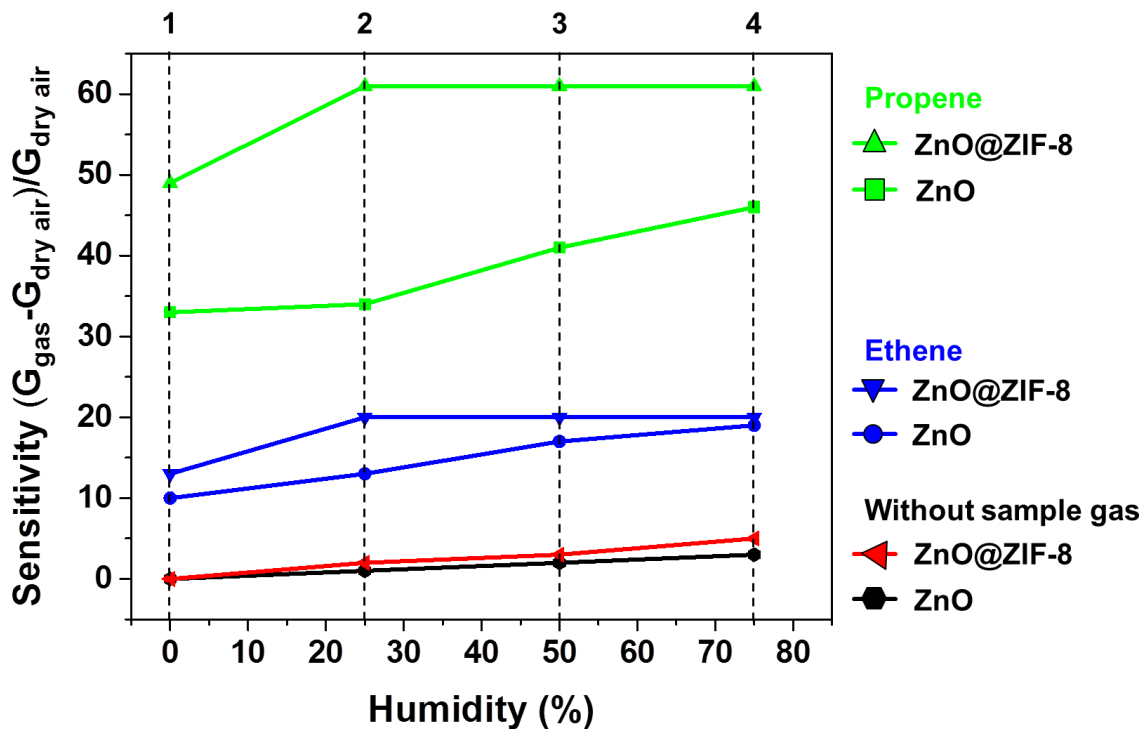


Figure 4: Sensitivity values to propene and ethene at 250 ppm, respectively, calculated according to Eq. 5 at those data points marked in Figs. 3a, 3c and 3d as a function of relative humidity. The numbers on top correspond to the numbers indicated in Fig. 3a, 3c and 3d. The conductance correlated to the corresponding air/sample gas mixture is generally recorded one hour after the change of gas composition without awaiting a stable signal state, i.e. the data shown in Fig. 4 reflect sensitivity trends.

In addition, Grand Canonical Monte Carlo (GCMC) calculations were carried out to simulate the adsorption of the different gaseous components (propene, ethene, oxygen, nitrogen, and water). The adsorption values of the different gases at the different experimental scenarios are summarized in Fig. S3. For details concerning the parameters and assumptions for the GCMC method see the experimental part of the supporting data.

4. Discussion

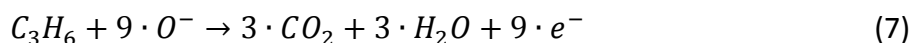
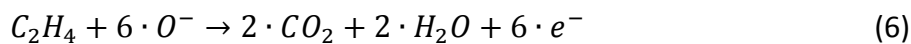
From Figs. 3c, 3d and 4 the following observations can be summarized: (i) For ZnO and ZnO@ZIF-8-based sensor types the conductance increased with propene or ethene gas exposure, reflecting typical n-type semiconductor behaviour [50] and a complete response recovery for both gases is observed. (ii) For both sensor materials a significantly higher sensitivity toward propene compared to that of ethene is measured (Fig.4). (iii) The conductance of the ZnO@ZIF-8-based sensing layer was measured to be generally higher

compared to the pure ZnO-layer (Fig. 3a, 3c and 3d). (iv) In the case of ZnO-based sensors (Fig. 3c) for both gases a stepwise increase in conductance due to a stepwise increase of rH from 25% to 75% is observed. This is in clear difference to the behaviour of the ZnO@ZIF-8-based gas sensor (Fig. 3d): Although for propene and ethene an increase of conductance can be observed after the initial step from rH=0% to rH=25%, no enhanced response to further rH increase is observed after some quick relaxation of the signal following the step of rH-change (Fig. 3d).

While several of the before mentioned observations such as the increase of the conductance of the gas sensitive material with increasing humidity or with target gas can be explained by Eqs. 1-4 in coincidence with the established theory of n-type gas sensors [51], the observation of no further change in sensitivity in the case of ZnO@ZIF-8-based sensor material when going from 25% rH to 50% rH or 75% rH (Fig. 3d) reflects an unexpected behaviour.

4.1 Sensitivity to propene and ethene

According to Fig. 4 both, ZnO- and ZnO@ZIF-8-based sensor materials exhibit a higher sensitivity towards propene than to ethene. One qualitative explanation for generally higher sensitivity to propene might be based on the assumption that a complete oxidation of the target gases at the ZnO/ZIF-8-interface takes place according to Eqs. 6 and 7. However, six oxygen atoms are consumed for one ethene molecule, while for propene molecule nine oxygen atoms are required, leading to the insertion of six, respectively nine electrons into the conduction band of ZnO and therefore the related conductance change is different. In this first approach of an explanation it is assumed that reactions (6) and (7) proceed with similar kinetics, i.e. the resulting O_{ads}^- surface fractional coverage which is given by the balance of reactions (1) and (2) and estimates the mobile electron concentration in the surface near the depletion layer of the ZnO is mainly estimated by the different numbers of electrons transferred per target molecule.



4.2 Influence of humidity

The particular phenomenon introduced in chapter 3 that an increase of humidity beyond 25% rH has no further influence on the **conductance** of the ZnO@ZIF-8-based material on target gases like propene and ethene, is now interpreted in several steps. First, the influence of (i) the sacrificially deposited ZIF-8 on ZnO and (ii) the humidity in the absence of sample gases on the conductance behaviour of the sensor is discussed. Fig. 3a shows the

conductance of the identical layer before (i.e. with pure ZnO, black line) and after the sacrificial deposition of ZIF-8 (i.e. with ZnO@ZIF-8, red line) in dependence on four different rH values (0%, 25%, 50%, 75%). After deposition of ZIF-8 the baseline conductance increased from $2.9 \cdot 10^{-5}$ S to $1.4 \cdot 10^{-4}$ S by a factor of about five. As this experiment was carried out with one and the same sensor chip before and after ZIF-8 coating and ZIF-8 itself was found to be a very good electrical insulator [52, 53], this considerable increase of conductance is explained by the increase of the electron density in the conduction band of the ZnO due to the ZIF-8 coating which is assumed to be correlated with the decrease of the adsorption site fractional coverage of O_{ads}^- surface states as a consequence of the change of the overall number of surface/interface states of the ZnO due to the degradation of the metal oxide during the sacrificial formation of the ZIF-8 shell. This hypothetical interpretation of the experimental results was not proven further in this study as the observed effects of adsorbed organic molecules or the surface roughness on the band gap of the ZnO-based semiconductors are well known [54-56].

When increasing rH to 25 % a significant increase in conductance can be observed for uncoated and coated ZnO (Fig. 3a). In case of uncoated ZnO the conductance increases by a factor of 7 from $2.9 \cdot 10^{-5}$ S (baseline) to $2.1 \cdot 10^{-4}$ S (peak conductance after rH increase) or by a factor of 3 when the conductance of $8.6 \cdot 10^{-5}$ S 1 h after rH increase and signal relaxation is taken into consideration. Correspondingly, for ZnO@ZIF-8 the conductance increases also by a factor of 7 from $1.4 \cdot 10^{-4}$ S (baseline) to $1.0 \cdot 10^{-3}$ S (peak conductance after rH increase). And again, when taking into account the conductance value of $4.7 \cdot 10^{-4}$ S 1 h after rH increase to 25% and signal relaxation, the increase factor of conductance for Zn@ZIF-8 is 3. This increase of conductance with increasing humidity is well-known from literature and is explained by different surface processes [5] where water interacts with the oxygen adsorbed on the metal oxide surface by forming hydroxyl groups. By this mechanism the electron which was trapped as a surface O_{ads}^- -state is transferred to the ZnO conduction band (Eq. 3). The sharp signal peak formation after humidity change especially when going from 0% rH to 25% rH indicates a quick surface process and a slower process of surface state formation and can less be explained by an assumed instability of gas exchange in the sensor cell.

4.3 Influence of humidity on the sensitivity to sample gas components

When increasing rH from 0% to 25 % after exposition of the target gases (250 ppm) propene and ethene, respectively, a significant increase in conductance only for ethene can be observed for both the uncoated and the coated ZnO (Figs. 3c and 3d), not for propene. Surprisingly and in disagreement with the observations to exposure with ethene, the conductance increase after exposition of 250 ppm propene is not observed when rH is set from 0% to 25% in the case of ZnO-based material (Fig. 3c). After a quick response, the conductance relaxes to approximately the same value which was reached at the step before

with the same propene concentration but 0% rH. This indicates, that at low water vapour partial pressure after signal relaxation there are no further electrons inserted into the ZnO conduction band compared with the relaxed situation at rH=0%.

Looking to ZnO@ZIF-8 the absolute increase of conductance when going from 0% rH to 25% rH is significantly higher at both target gases (250 ppm) compared to that of ZnO (Figs. 3c and 3d). And, in case of ethene exposure, the relative increase of conductance is not so much different for both materials (Fig. 4) showing that the coating with ZIF-8 results mainly in an offset by more than an order of magnitude related to the conductance values obtained with ZnO without MOF coating. These observations, however, mean that ZIF-8 does not significantly hinder water diffusion to the ZnO/ZIF-8-interface, although ZIF-8 is known as a hydrophobic material [57]. We have to take into consideration that the permeation of any gas through a membrane includes three steps: (1) the sorption of the gas at the solid interface, (2) the diffusion of the gas inside or through the pores of the membrane material and (3) the desorption from the opposite membrane surface to the gas phase [58]. The Grand Canonical Monte Carlo (GCMC) method was used in this work to simulate the adsorption of the different gases involved in the sensor experiments including O₂, N₂, H₂O, propene and ethene as a function of humidity (Fig. S3). According to the results it is obvious that the uptake of water in ZIF-8 (i.e. less than 0.09 cm³ H₂O/cm³ ZIF-8) is negligible compared to the uptake of the other gases. This is in agreement with results from Zhang *et al.* [59] where single-component adsorption isotherms for water and ethanol in ZIF-8 were determined. However, when comparing the corrected diffusivity for water at 40 °C (1.8×10^{-7} [59]) with the corrected diffusivities for the other gases such as propene ($3.6 \pm 1.6 \times 10^{-7}$ [60]) or ethene ($1.6 \pm 0.3 \times 10^{-8}$ [60]) at 35 °C it can be concluded that the diffusivity for water is comparable or even higher than those for the organic gases used in our work. This finding is supported by the work of Han *et al.* that mentions point defects in the ZIF-8 framework as origin of this increased diffusivity for water despite the hydrophobic character of the MOF material, particularly the hydrophobic character of the imidazole linker molecules. They used molecular simulations by introducing a force field which implements point defects in the ZIF-8 structure and determined a value for the self-diffusion coefficients D_{self} for water of $2.5 \cdot 10^{-5}$ cm²·s⁻¹ [61]. The D_{self} value of water experimentally determined by Zhang *et al.* is $1.0 \cdot 10^{-5}$ cm²·s⁻¹ [59] and is in good agreement with the theory values. Compared to simulated D_{self} values for ethene ($D_{\text{self}} = 4 \cdot 10^{-7}$ cm²·s⁻¹ [62]) or propene ($D_{\text{self}} = 2 \cdot 10^{-10}$ cm²·s⁻¹ [62]) the self-diffusion coefficient of water is significantly higher than those of the alkenes which is qualitatively in agreement with the findings for the corrected diffusivities mentioned above.

As already mentioned above, in the case of ZnO-based material there is a clear increase of the conductivity with relative humidity at values beyond rH=25% (Fig. 3c), while for the ZnO@ZIF-8-based sensitive layer a conductivity increase is only observable when going from 0% to 25% rH. This behaviour of the ZnO@ZIF-8 gas sensitive layer in the presence of sample gases propene and ethene (Fig. 3d) is different compared to the case, when no sample gases

are present (Fig. 3a), where a clear increase of conductance was observed with each step of humidity increase. In this context the GCMC results (Fig. S3) of the sample gases can help to understand this behaviour. As mentioned above water shows a high self-diffusion coefficient for the ZIF-8 framework. However, this diffusion could be significantly hindered, when other gases are present, which show a strong adsorption to ZIF-8 framework. Figs. S3a and S3b show that the calculated adsorption of the sample gases propene (26 cm^3 per cm^3 ZIF-8) and ethene (2.6 cm^3 per cm^3 ZIF-8) are significantly higher than that of water and that the adsorption of propene is about ten times higher than that of ethene. When looking at the values for experimentally determined permeabilities for both gases the values vary between 994 Barrer (measured at $23 \text{ }^\circ\text{C}$) [63] and 1270 Barrer (measured at $23 \text{ }^\circ\text{C}$) [64] for ethene and 201 Barrer [65] and 390 Barrer (both measured at $35 \text{ }^\circ\text{C}$) [62] for propene. Here the permeability of ethene is up to a factor of 6 higher than that of propene. Due to the fact that the sorption of ethene is just 10% of that of propene this means that for ethene the permeability is dominated by diffusion.

With the arguments mentioned so far, we now can conclude: (i) By coating with ZIF-8 the conductance of the ZnO-layer is enhanced by about a factor of 4 (Fig. 3a) at synthetic air conditions (base line). As we can exclude that electrons from the electrically insulating ZIF-8 are injected into the conduction band of the ZnO electron depletion layer, consequently it has to be concluded, that the density of reaction sites, here especially the O_{ads}^- surface state density, is reduced at the ZnO/ZIF-8-interface by the ZIF-8 covering process which could explain the observed conductance increase. (ii) The initial increase of the sensor conductance when dosing the corresponding sample gas at $\text{rH}=0\%$ (Figs. 3c and 3d) is interpreted to be observed due to the further decrease of O_{ads}^- adsorption sites in general accordance with the gas sensing behaviour of n-type metal oxide materials in accordance with eq. 2. In addition, when comparing the absolute values of conductance of ZnO and ZnO@ZIF-8 based material after exposition of the target gas as shown in Figs. 3c and 3d, respectively, in the latter case we find values which are up to 30 times higher than those for ZnO. This can be explained by the fact that the water molecules produced at the surface/interface according to Eq. 4 in case of ZnO can desorb from the surface and equilibrate with the adjacent atmosphere. In contrast in case of ZnO@ZIF-8 the water molecules are “trapped” at the ZnO/ZIF-8 interface as the SURMOF acts like a diffusion barrier. It was shown above by literature [64, 65] and by our theoretical results (see supporting information) that the desorption of the water (as a reaction product) is hindered by the ZIF-8 coating when ethene or propene are present. This explains the increase in activity of water molecules at the interface of ZnO/ZIF-8 and, therefore, the formation of additional OH_{ads} states which consequently should result in an increased conductance according to Eq. 3 in full agreement with the data (compare Fig. 3c with Fig. 3d). (iii) When increasing the rH to 25%, in case of ZnO after relaxation there is no conductance increase measured at propene and only a slight increase observed at ethene exposure. But, surprisingly, the corresponding conductance change of the ZnO@ZIF-8-layer is much higher

(Fig. 3b,c and Fig. 4). Further increase of rH to 50% and 75% induces further stepwise increase of conductance at ZnO but leads to a conductance saturation effect in case of ZnO@ZIF-8, i.e. the sensitivity to water vapour is limited at the ZIF-8 coated ZnO-layer. In a first attempt of interpretation the enhanced sensitivity of the ZnO/ZIF-8-interface to rH at the step from 0% rH to 25% rH may be due to the above mentioned hindering of desorption of the water molecules which leads to enhanced formation of OH_{ads} surface states related to the corresponding conductance increase (Eq. 3). The saturation of sensitivity to water vapour at further rH-increase in presence of the target gases may be due to the saturation of the OH_{ads} reaction sites at the ZnO/ZIF-8-interface (Fig. 3d) which may be a consequence of (i) a limited/reduced number of total reaction sites (reduced density of O_{ads}^- surface states, argument already stated in this paragraph above) and (ii) hindering of free exchange of water molecules with the atmosphere by the ZIF-8 coating. In contrast to ZnO@ZIF-8-based material, pure ZnO (Figs. S3c and S3d) shows a significant dependence on humidity. According to the GCMC calculations (Figs. S3c and S3d), the adsorption of water is significantly higher by a factor of about 5×10^3 compared to that of propene or ethene. From that we can conclude that the conductivity is particularly influenced by the dynamic equilibrium of adsorption and desorption of the H_2O molecules coming from the surrounding atmosphere while the influence of water produced by the surface reaction of the sample gases plays only a minor role.

5. Conclusion

ZnO@ZIF-8 core-shell heterostructures have been fabricated on thin-film Pt-interdigitated electrodes (IDEs), following a self-sacrificial template assisted synthesis. The gas sensing behaviour towards propene and ethene has been studied under non-humid and humid atmosphere conditions. The structural and morphological analysis supported the formation of core-shell heterostructures with a functional ZnO core and a porous ZIF-8 shell and good material stability under the given experimental conditions. Gas sensing tests yielded an increased sensitivity towards propene compared to that of ethene, a general increase of conductance after deposition of ZIF-8 and a typical sensitivity of both, the ZnO- and the ZnO@ZIF-8 layer to water vapour when exposed to synthetic air. However, at exposure to the target gases the conductance of the ZnO@ZIF-8-layer increased with increase of the relative humidity to 25%, while a further increase of rH does affect neither the conductivity nor the sensitivity of the sensor. An explanation approach for this unexpected behaviour is based (i) on comparable gas sensitivity experiments to propene and ethene at various relative humidities of the identical ZnO-layer uncoated and after coating with ZIF-8 and (ii) on comparative calculations of the adsorption properties of all included gas components in the ZIF-8 pores and on the ZnO surface by Grand Canonical Monte Carlo simulations assuming the experimental conditions. The experimental results have been interpreted by assuming that the gas sensitivity of the ZnO@ZIF-8 layer is given by gas reaction processes

at the interface between ZnO and ZIF-8. In this context it is an interesting and important result that in spite of the insulating properties of ZIF-8 there is a clear increase of conductivity of the ZnO@ZIF-8 layer. This was interpreted by the coating process induced reduction of the density of surface reaction sites, which limits the formation of O_{ads}^- and OH_{ads} states and takes corresponding influence on the conductivity behavior.

The fact that the sensitivity of a metal oxide based sensor is independent of relative humidity after exceeding 25% rH threshold (21°C), is highly relevant from an application point of view having in mind, that the cross-sensitivity to humidity is one of the most problematic and challenging properties of those types of metal oxide gas sensors.

Overall, the results of this work are promising in terms of developing metal oxide based gas sensors which are not only stable against water vapour and high operation temperatures up to 400°C but which also show a significantly reduced dependence of the sensor performance on relative humidity. A future challenge will be the improvement of the sensors in terms of response time which can be realized e.g. by optimizing the thickness of the ZIF-8 layer and the investigation of sensitivity behaviour in case of multi-component gas mixtures.

Acknowledgement

SSN, NI, CW, HK, and HG thank the Baden-Württemberg Stiftung gGmbH for financial support within the project CT-7 of the CleanTech Initiative. We gratefully acknowledge the discussions with Dr. Elvia Valadez-Sánchez concerning the diffusion of gases through ZIF-8 frameworks.

References

- [1] G. Heiland, Zum Einfluß von Wasserstoff auf die elektrische Leitfähigkeit an der Oberfläche von Zinkoxydkristallen, *Z. Phys.* (1957) 15-27. <https://doi.org/10.1007/bf01327362>.
- [2] T. Seiyama, A. Kato, K. Fujiishi, M. Nagatani, A New Detector for Gaseous Components Using Semiconductive Thin Films, *Anal. Chem.* (1962) 1502-1503. <https://doi.org/10.1021/ac60191a001>.
- [3] S. R. Morrison, Selectivity in semiconductor gas sensors, *Sensor Actuator* (1987) 425-440. [https://doi.org/10.1016/0250-6874\(87\)80061-6](https://doi.org/10.1016/0250-6874(87)80061-6).
- [4] S. R. Morrison, Semiconductor gas sensors, *Sensor Actuator* (1981) 329-341. [https://doi.org/10.1016/0250-6874\(81\)80054-6](https://doi.org/10.1016/0250-6874(81)80054-6).
- [5] N. Bârsan, U. Weimar, Understanding the fundamental principles of metal oxide based gas sensors; the example of CO sensing with SnO₂ sensors in the presence of humidity, *J. Phys. Condens. Mat.* (2003) R813. <http://stacks.iop.org/0953-8984/15/i=20/a=201>.
- [6] D. Koziej, N. Bârsan, U. Weimar, J. Szuber, K. Shimanoe, N. Yamazoe, Water–oxygen interplay on tin dioxide surface: Implication on gas sensing, *Chem. Phys. Lett.* (2005) 321-323. <https://doi.org/10.1016/j.cplett.2005.05.107>.
- [7] P. T. Moseley, Progress in the development of semiconducting metal oxide gas sensors: a review, *Meas. Sci. Technol.* (2017). 082001. <https://doi.org/10.1088/1361-6501/aa7443>.
- [8] Z. Yalei, Z. Wenlong, Y. Bin, L. Jingquan, C. Xiang, W. Xiaolin, Y. Chunsheng, Gas-sensing enhancement methods for hydrothermal synthesized SnO₂ -based sensors, *Nanotechnology* (2017) 452002. <https://doi.org/10.1088/1361-6528/aa86a2>.
- [9] A. Vergara, E. Llobet, J. Brezmes, P. Ivanov, C. Cané, I. Gràcia, X. Vilanova, X. Correig, Quantitative gas mixture analysis using temperature-modulated micro-hotplate gas sensors: Selection and validation of the optimal modulating frequencies, *Sens. Actuator B Chem.* (2007) 1002-1016. <https://doi.org/10.1016/j.snb.2006.11.010>.
- [10] M. A. Andio, P. N. Browning, P. A. Morris, S. A. Akbar, Comparison of gas sensor performance of SnO₂ nano-structures on microhotplate platforms, *Sens. Actuator B Chem.* (2012) 13-18. <https://doi.org/10.1016/j.snb.2011.12.045>.
- [11] R. Mohammadzadeh Kakhki, Recent developments on application of nanometal-oxide based gas sensor arrays, *Russ. J. Appl. Chem.* (2017) 1030-1039. <https://doi.org/10.1134/s1070427217070023>.
- [12] R. Seifert, H. B. Keller, N. Illyaskutty, J. Knoblauch, H. Kohler, Numerical Signal Analysis of Thermo-Cyclically Operated MOG Gas Sensor Arrays for Early Identification of Emissions from Overloaded Electric Cables, *Sensors and Transducers* (2015) 6. http://www.sensorsportal.com/HTML/DIGEST/P_2738.htm.
- [13] N. Illyaskutty, J. Knoblauch, M. Schwotzer, H. Kohler, Thermally modulated multi sensor arrays of SnO₂/additive/electrode combinations for enhanced gas identification, *Sens. Actuator B Chem.* (2015) 2-12. <https://doi.org/10.1016/j.snb.2015.03.018>.

- [14] J. Lee, J. H. Kwak, W. Choe, Evolution of form in metal–organic frameworks, *Nat. Commun.* (2017) 14070. <https://doi.org/10.1038/ncomms14070>.
- [15] Y. Liu, Z. Tang, Multifunctional Nanoparticle@MOF Core–Shell Nanostructures, *Multifunctional Nanoparticle@MOF Core–Shell Nanostructures* (2013) 5819-5825. <https://doi.org/10.1002/adma.201302781>.
- [16] Q. Yang, W. Liu, B. Wang, W. Zhang, X. Zeng, C. Zhang, Y. Qin, X. Sun, T. Wu, J. Liu, F. Huo, J. Lu, Regulating the spatial distribution of metal nanoparticles within metal-organic frameworks to enhance catalytic efficiency, *Nat. Commun.* (2017) 14429. <https://doi.org/10.1038/ncomms14429>.
- [17] M. Zeng, Z. Chai, X. Deng, Q. Li, S. Feng, J. Wang, D. Xu, Core–shell CdS@ZIF-8 structures for improved selectivity in photocatalytic H₂ generation from formic acid, *Nano Res.* (2016) 2729-2734. <https://doi.org/10.1007/s12274-016-1161-3>.
- [18] R. Kaur, K.-H. Kim, A. K. Paul, A. Deep, Recent advances in the photovoltaic applications of coordination polymers and metal organic frameworks, *J. Mater. Chem. A* (2016) 3991-4002. <https://doi.org/10.1039/C5TA09668E>.
- [19] D. Y. Lee, C. Y. Shin, S. J. Yoon, H. Y. Lee, W. Lee, N. K. Shrestha, J. K. Lee, S.-H. Han, Enhanced photovoltaic performance of Cu-based metal-organic frameworks sensitized solar cell by addition of carbon nanotubes, *Sci. Rep. UK* (2014) 3930. <https://doi.org/10.1038/srep03930>.
- [20] X. Ge, Z. Li, C. Wang, L. Yin, Metal–Organic Frameworks Derived Porous Core/Shell Structured ZnO/ZnCo₂O₄/C Hybrids as Anodes for High-Performance Lithium-Ion Battery, *ACS Appl. Mater. Interfaces* (2015) 26633-26642. <https://doi.org/10.1021/acsami.5b08195>.
- [21] Y. Han, P. Qi, J. Zhou, X. Feng, S. Li, X. Fu, J. Zhao, D. Yu, B. Wang, Metal–Organic Frameworks (MOFs) as Sandwich Coating Cushion for Silicon Anode in Lithium Ion Batteries, *ACS Appl. Mater. Interfaces* (2015) 26608-26613. <https://doi.org/10.1021/acsami.5b08109>.
- [22] A. Magasinski, P. Dixon, B. Hertzberg, A. Kvit, J. Ayala, G. Yushin, High-performance lithium-ion anodes using a hierarchical bottom-up approach, *Nat. Mater.* (2010) 353. <https://doi.org/10.1038/nmat2725>.
- [23] T. Li, J. E. Sullivan, N. L. Rosi, Design and Preparation of a Core–Shell Metal–Organic Framework for Selective CO₂ Capture, *J. Am. Chem. Soc.* (2013) 9984-9987. <https://doi.org/10.1021/ja403008j>.
- [24] D. K. Panchariya, R. K. Rai, E. Anil Kumar, S. K. Singh, Core–Shell Zeolitic Imidazolate Frameworks for Enhanced Hydrogen Storage, *Core–Shell Zeolitic Imidazolate Frameworks for Enhanced Hydrogen Storage* (2018) 167-175. <https://doi.org/10.1021/acsomega.7b01693>.
- [25] W. Cho, H. J. Lee, S. Choi, Y. Kim, M. Oh, Highly effective heterogeneous chemosensors of luminescent silica@coordination polymer core-shell micro-structures for metal ion sensing, *Sci. Rep. UK* (2014) 6518. <https://doi.org/10.1038/srep06518>.
- [26] D.-X. Xue, Y. Belmabkhout, O. Shekhah, H. Jiang, K. Adil, A. J. Cairns, M. Eddaoudi, Tunable Rare Earth fcu-MOF Platform: Access to Adsorption Kinetics Driven Gas/Vapor Separations via Pore Size Contraction, *J. Am. Chem. Soc.* (2015) 5034-5040. <https://doi.org/10.1021/ja5131403>.
- [27] O. M. Yaghi, G. M. Li, H. L. Li, SELECTIVE BINDING AND REMOVAL OF GUESTS IN A MICROPOROUS METAL-ORGANIC FRAMEWORK, *Nature* (1995) 703-706. <https://doi.org/10.1038/378703a0>.
- [28] J. Liu, C. Woll, Surface-supported metal-organic framework thin films: fabrication methods, applications, and challenges, *Chem. Soc. Rev.* (2017) 5730-5770. <https://doi.org/10.1039/c7cs00315c>.
- [29] M. Drobek, J.-H. Kim, M. Bechelany, C. Vallicari, A. Julbe, S. S. Kim, MOF-Based Membrane Encapsulated ZnO Nanowires for Enhanced Gas Sensor Selectivity, *ACS Appl. Mater. Interfaces* (2016) 8323-8328. <https://doi.org/10.1021/acsami.5b12062>.

- [30] H. Tian, H. Fan, M. Li, L. Ma, Zeolitic Imidazolate Framework Coated ZnO Nanorods as Molecular Sieving to Improve Selectivity of Formaldehyde Gas Sensor, *Zeolitic Imidazolate Framework Coated ZnO Nanorods as Molecular Sieving to Improve Selectivity of Formaldehyde Gas Sensor* (2016) 243-250. [10.1021/acssensors.5b00236](https://doi.org/10.1021/acssensors.5b00236).
- [31] M.-S. Yao, W.-X. Tang, G.-E. Wang, B. Nath, G. Xu, MOF Thin Film-Coated Metal Oxide Nanowire Array: Significantly Improved Chemiresistor Sensor Performance, *Adv. Mater.* (2016) 5229-5234. <https://doi.org/10.1002/adma.201506457>.
- [32] W.-w. Zhan, Q. Kuang, J.-z. Zhou, X.-j. Kong, Z.-x. Xie, L.-s. Zheng, Semiconductor@Metal–Organic Framework Core–Shell Heterostructures: A Case of ZnO@ZIF-8 Nanorods with Selective Photoelectrochemical Response, *J. Am. Chem. Soc.* (2013) 1926-1933. <https://doi.org/10.1021/ja311085e>.
- [33] N. Zhang, B. Zhu, F. Peng, X. Yu, Y. Jia, J. Wang, L. Kong, Z. Jin, T. Luo, J. Liu, Synthesis of metal-organic-framework related core-shell heterostructures and their application to ion enrichment in aqueous conditions, *Chem. Commun.* (2014) 7686-7689. <https://doi.org/10.1039/c4cc00900b>.
- [34] N. Barsan, M. Schweizer-Berberich, W. Göpel†, Fundamental and practical aspects in the design of nanoscaled SnO₂ gas sensors: a status report, *Fresen. J. Anal. Chem.* (1999) 287-304. <https://doi.org/10.1007/s002160051490>.
- [35] B. Ojha, N. Illyaskutty, J. Knoblauch, M. R. Balachandran, H. Kohler, High-temperature CO / HC gas sensors to optimize firewood combustion in low-power fireplaces, *J. Sens. Sens. Syst.* (2017) 237-246. <https://doi.org/10.5194/jsss-6-237-2017>.
- [36] E. P. V. Sanchez, H. Gliemann, K. Haas-Santo, C. Woll, R. Dittmeyer, ZIF-8 SURMOF Membranes Synthesized by Au-Assisted Liquid Phase Epitaxy for Application in Gas Separation, *Chem. Ing. Tech.* (2016) 1798-1805. <https://doi.org/10.1002/cite.201600061>.
- [37] K. S. Park, Z. Ni, A. P. Côté, J. Y. Choi, R. Huang, F. J. Uribe-Romo, H. K. Chae, M. O’Keeffe, O. M. Yaghi, Exceptional chemical and thermal stability of zeolitic imidazolate frameworks, *P. Natl. Acad. Sci. USA* (2006) 10186. <https://doi.org/10.1073/pnas.0602439103>.
- [38] O. Shekhah, H. Wang, S. Kowarik, F. Schreiber, M. Paulus, M. Tolan, C. Sternemann, F. Evers, D. Zacher, R. A. Fischer, C. Woll, Step-by-step route for the synthesis of metal-organic frameworks, *J. Am. Chem. Soc.* (2007) 15118-15119. <https://doi.org/10.1021/ja076210u>.
- [39] H. K. Arslan, O. Shekhah, J. Wohlgemuth, M. Franzreb, R. A. Fischer, C. Woll, High-Throughput Fabrication of Uniform and Homogenous MOF Coatings, *Adv. Funct. Mater.* (2011) 4228-4231. <https://doi.org/10.1002/adfm.201101592>.
- [40] Z. Feng, H. Xianluo, L. Zhen, Q. Long, H. Chenchen, Z. Rui, J. Yan, H. Yunhui, MOF-Derived Porous ZnO/ZnFe₂O₄/C Octahedra with Hollow Interiors for High-Rate Lithium-Ion Batteries, *Adv. Mater.* (2014) 6622-6628. <https://doi.org/10.1002/adma.201402322>.
- [41] E. Zanchetta, L. Malfatti, R. Ricco, M. J. Styles, F. Lisi, C. J. Coghlan, C. J. Doonan, A. J. Hill, G. Brusatin, P. Falcaro, ZnO as an Efficient Nucleating Agent for Rapid, Room Temperature Synthesis and Patterning of Zn-Based Metal–Organic Frameworks, *Chem. Mater.* (2015) 690-699. <https://doi.org/10.1021/cm502882a>.
- [42] J. Knoblauch, N. Illyaskutty, H. Kohler, Early detection of fires in electrical installations by thermally modulated SnO₂/additive-multi sensor arrays, *Sens. Actuator B Chem.* (2015) 36-40. <https://doi.org/10.1016/j.snb.2015.02.014>.
- [43] K. Frank, V. Magapu, V. Schindler, H. Kohler, H. B. Keller, R. Seifert, Chemical Analysis with Tin Oxide Gas Sensors: Choice of Additives, Method of Operation and Analysis of Numerical Signal, *Sens. Lett.* (2008) 908-911. <https://doi.org/10.1166/sl.2008.527>.
- [44] Z. Han, S. Li, J. Chu, Y. Chen, Controlled growth of well-aligned ZnO nanowire arrays using the improved hydrothermal method, *J. Semicond.* (2013) 063002. <https://doi.org/10.1088/1674-4926/34/6/063002>.

- [45] S. Li, W. Zhang, Y. Zhu, Q. Zhao, F. Huo, Synthesis of MOFs and Their Composite Structures through Sacrificial-Template Strategy, *Cryst. Growth Des.* (2015) 1017-1021. <https://doi.org/10.1021/cg501551y>.
- [46] X. Wu, S. Xiong, Z. Mao, S. Hu, X. Long, A Designed ZnO@ZIF-8 Core–Shell Nanorod Film as a Gas Sensor with Excellent Selectivity for H₂ over CO, *Chem. Eur. J.* (2017) 7969-7975. <https://doi.org/10.1002/chem.201700320>.
- [47] N. Illyaskutty, H. Kohler, T. Trautmann, M. Schwotzer, V. P. M. Pillai, Enhanced ethanol sensing response from nanostructured MoO₃:ZnO thin films and their mechanism of sensing, *J. Mater. Chem. C* (2013) 3976-3984. <https://doi.org/10.1039/c3tc30408f>.
- [48] A. Jerger, H. Kohler, F. Becker, H. B. Keller, R. Seifert, New applications of tin oxide gas sensors: II. Intelligent sensor system for reliable monitoring of ammonia leakages, *Sens. Actuator B Chem.* (2002) 301-307. [https://doi.org/10.1016/S0925-4005\(01\)00970-4](https://doi.org/10.1016/S0925-4005(01)00970-4).
- [49] K. Fujie, K. Otsubo, R. Ikeda, T. Yamada, H. Kitagawa, Low temperature ionic conductor: ionic liquid incorporated within a metal–organic framework, *Chem. Sci.* (2015) 4306-4310. <https://doi.org/10.1039/c5sc01398d>.
- [50] J. Gong, Q. Chen, M.-R. Lian, N.-C. Liu, R. G. Stevenson, F. Adami, Micromachined nanocrystalline silver doped SnO₂ H₂S sensor, *Sens. Actuator B Chem.* (2006) 32-39. <https://doi.org/10.1016/j.snb.2005.04.035>.
- [51] C. Wang, L. Yin, L. Zhang, D. Xiang, R. Gao, Metal Oxide Gas Sensors: Sensitivity and Influencing Factors, *Metal Oxide Gas Sensors: Sensitivity and Influencing Factors* (2010) 2088-2106. 10.3390/s100302088.
- [52] S. Eslava, L. Zhang, S. Esconjauregui, J. Yang, K. Vanstreels, M. R. Baklanov, E. Saiz, Metal-Organic Framework ZIF-8 Films As Low-κ Dielectrics in Microelectronics, *Chem. Mater.* (2013) 27-33. <https://doi.org/10.1021/cm302610z>.
- [53] E.-X. Chen, H. Yang, J. Zhang, Zeolitic Imidazolate Framework as Formaldehyde Gas Sensor, *Inorg. Chem.* (2014) 5411-5413. <https://doi.org/10.1021/ic500474j>.
- [54] J. Herrán, I. Fernández, R. Tena-Zaera, E. Ochoteco, G. Cabañero, H. Grande, Schottky diodes based on electrodeposited ZnO nanorod arrays for humidity sensing at room temperature, *Sens. Actuator B Chem.* (2012) 274-278. <https://doi.org/10.1016/j.snb.2012.08.009>.
- [55] J. Gamon, D. Giaume, G. Lefèvre, T. Le Mercier, P. Barboux, The effect of organic additives on the intergranular conductivity of Al-doped ZnO, *The effect of organic additives on the intergranular conductivity of Al-doped ZnO* (2017) 38019-38027. 10.1039/c7ra02975f.
- [56] R. S. Gaikwad, S. S. Bhande, R. S. Mane, B. N. Pawar, S. L. Gaikwad, S.-H. Han, O.-S. Joo, Roughness-based monitoring of transparency and conductivity in boron-doped ZnO thin films prepared by spray pyrolysis, *Mater. Res. Bull.* (2012) 4257-4262. <https://doi.org/10.1016/j.materresbull.2012.09.022>.
- [57] K. Zhang, R. P. Lively, C. Zhang, W. J. Koros, R. R. Chance, Investigating the Intrinsic Ethanol/Water Separation Capability of ZIF-8: An Adsorption and Diffusion Study, *J. Phys. Chem. C* (2013) 7214-7225. <https://doi.org/10.1021/jp401548b>.
- [58] B. Flaconneche, J. Martin, M. H. Klopffer, Permeability, Diffusion and Solubility of Gases in Polyethylene, Polyamide 11 and Poly (Vinylidene Fluoride), *Oil Gas Sci. Technol.* (2001) 261-278. <https://doi.org/10.2516/ogst:2001023>.
- [59] K. Zhang, R. P. Lively, C. Zhang, R. R. Chance, W. J. Koros, D. S. Sholl, S. Nair, Exploring the Framework Hydrophobicity and Flexibility of ZIF-8: From Biofuel Recovery to Hydrocarbon Separations, *J. Phys. Chem. Lett.* (2013) 3618-3622. <https://doi.org/10.1021/jz402019d>.
- [60] R. J. Verploegh, S. Nair, D. S. Sholl, Temperature and Loading-Dependent Diffusion of Light Hydrocarbons in ZIF-8 as Predicted Through Fully Flexible Molecular Simulations, *J. Am. Chem. Soc.* (2015) 15760-15771. <https://doi.org/10.1021/jacs.5b08746>.
- [61] C. Han, R. J. Verploegh, D. S. Sholl, Assessing the Impact of Point Defects on Molecular Diffusion in ZIF-8 Using Molecular Simulations, *J. Phys. Chem. Lett.* (2018) 4037-4044. <https://doi.org/10.1021/acs.jpcllett.8b01749>.

- [62] C. Zhang, R. P. Lively, K. Zhang, J. R. Johnson, O. Karvan, W. J. Koros, Unexpected Molecular Sieving Properties of Zeolitic Imidazolate Framework-8, *J. Phys. Chem. Lett.* (2012) 2130-2134. <https://doi.org/10.1021/jz300855a>.
- [63] Y. Pan, Z. Lai, Sharp separation of C2/C3 hydrocarbon mixtures by zeolitic imidazolate framework-8 (ZIF-8) membranes synthesized in aqueous solutions, *Chem. Commun.* (2011) 10275-10277. <https://doi.org/10.1039/c1cc14051e>.
- [64] H. Bux, C. Chmelik, R. Krishna, J. Caro, Ethene/ethane separation by the MOF membrane ZIF-8: Molecular correlation of permeation, adsorption, diffusion, *J. Membrane Sci.* (2011) 284-289. <https://doi.org/10.1016/j.memsci.2010.12.001>.
- [65] A. J. Brown, N. A. Brunelli, K. Eum, F. Rashidi, J. R. Johnson, W. J. Koros, C. W. Jones, S. Nair, Interfacial microfluidic processing of metal-organic framework hollow fiber membranes, *Science* (2014) 72-75. <https://doi.org/10.1126/science.1251181>.

ZnO@ZIF-8: Gas sensitive core-shell hetero-structures show reduced cross-sensitivity to humidity

Sreeja Sreedharan Nair^{1,}, Navas Illyaskutty^{2,*}, Benjamin Tam³, A. Ozgur Yazaydin³, Katja Emmerich⁴, Annett Steudel⁴, Tawheed Hashem¹, Ludger Schöttner¹, Christof Wöll¹, Heinz Kohler^{2,#}, Hartmut Gliemann^{1,§}*

¹*Institute of Functional Interfaces (IFG), Karlsruhe Institute of Technology (KIT), Hermann-von-Helmholtz Platz-1, 76344 Eggenstein-Leopoldshafen, Germany*

²*Institute for Sensor and Information Systems (ISIS), Hochschule Karlsruhe – Technik und Wirtschaft, Moltkestr. 30, 76133 Karlsruhe, Germany*

³*Department of Chemical Engineering, University College London, Torrington Place, London WC1E 7JE, United Kingdom*

⁴*Center of Material Moisture (CMM), Karlsruhe Institute of Technology (KIT), Hermann-von-Helmholtz Platz-1, 76344 Eggenstein-Leopoldshafen, Germany*

**Both authors contributed equally*

Corresponding authors: §hartmut.gliemann@kit.edu, #heinz.kohler@hs-karlsruhe.de

Supporting information

- 1. Characterization of ZnO- and ZnO@ZIF-8-based sensor material by XRD (p. 2)**
- 2. Characterization of ZnO- and ZnO@ZIF-8-based sensor material by XPS (p. 3)**
- 3. Characterization of ZnO- and ZnO@ZIF-8-based sensor material by simultaneous thermal analysis (p. 5)**
- 4. Grand Canonical Monte Carlo (GCMC) method for calculating adsorption isotherms (p. 7)**

1. Characterization of ZnO- and ZnO@ZIF-8-based sensor material by XRD

X-ray diffraction (XRD) measurements in out-of-plane geometry were carried out with a Bruker D8-Advance diffractometer using Cu $K_{\alpha 1}$ radiation ($\lambda=0.154$ nm). For additional prove of the co-existence of the ZnO and the crystalline ZIF-8 phase in case of ZnO@ZIF-8 XRD was carried out with pure ZnO nanopillars (black curve in Figure S1a) and with ZnO pillars coated with ZIF-8 (blue curve in Figure S1a). The red curve in Figure S1a represents the simulated XRD pattern of ZIF-8. The strong reflexes of ZnO can also be detected in the case of ZnO@ZIF-8. The reflexes of the simulated ZIF-8 XRD pattern are in agreement with those of ZnO@ZIF-8 [1]. XRD investigation after the sensing experiment with different gases and humidity values show no change in the diffractogram (Fig. S1b).

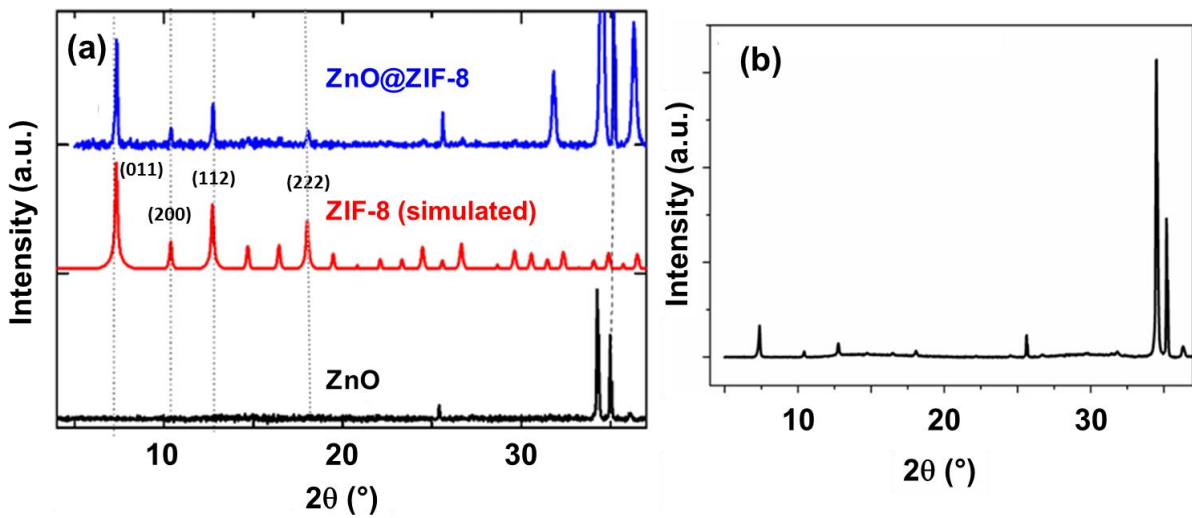


Figure S1: (a) shows the XRD patterns of ZnO nanostructures grown on IDE (black); simulated XRD pattern of ZIF-8 (red) and ZnO@ZIF-8 gas sensors (blue); (b) shows the XRD pattern of ZnO@ZIF-8 after the measurement with probe gases.

2. Characterization of ZnO- and ZnO@ZIF-8-based sensor material by XPS

XPS analyses further substantiate the partial conversion of ZnO to ZnO@ZIF-8 composite material. The high resolution XPS 2p spectrum of Zn shows two characteristic peaks at 1045.85 eV and 1022.75 eV (Fig. S1a) which can be assigned to the $2p_{1/2}$ and $2p_{3/2}$ binding energies of Zn^{2+} [2, 3]. In addition, the binding energies of N 1s (Fig. S1b) and C 1s peaks (Fig. S1c) are observed at 398.5 eV, and 285.5 eV, respectively, which are characteristic for the imidazole linker [4, 5].

XPS analyses further substantiate the partial conversion of ZnO to ZnO@ZIF-8 composite material. Here we show the corresponding XP spectra, which were resolved on C 1s (Fig. S2a), N 1s (Fig. S2b) and Zn 2p (Fig. S2c) binding energy regions.

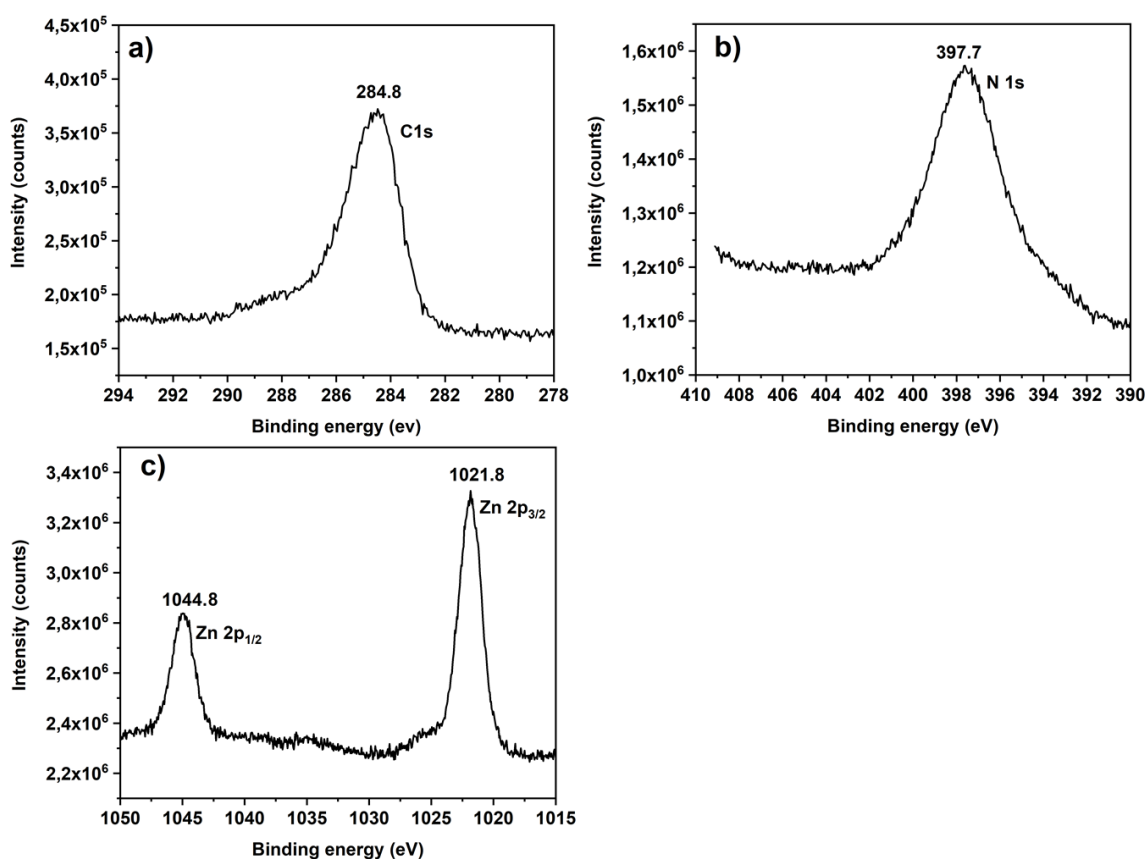


Figure S2: (a) C 1s, (b) N 1s and (c) Zn 2p XPS data of the ZnO@ZIF-8 based sensor material.

Before measurement, the sample was vacuum dried overnight. The spectra were recorded under grazing emission ($\theta=70^\circ$) with Al K_α radiation at room temperature. The binding energies of all elemental components were calibrated on the main carbon line at 284.8 eV. According to literature this peak can be associated to the carbon atoms of the pentagonal ring from imidazolate units, which all exhibit sp^2 -character [6]. The shoulder around 288.5 eV could be related to the presence of carbonate or carboxylate terminations, which may decorate

the surface of the ZIF-8 framework [7, 8]. In compatibility to literature the N 1s peak was identified at 397.7 eV and characterizes both of the N-heteroatoms in the 2-methylimidazole linker [9, 10]. It is worth to mention, that the satellite feature around the position of 394.1 eV does not belong to the MOF compound itself. Instead, it is attributed to an unwanted molybdenum (Mo 2p_{3/2}) contaminant that was unfortunately measured along the sample carrier. This is confirmed by the spectrum of the full range survey. Finally, the high resolution XPS 2p spectrum of Zn shows peaks at 1044.8 eV and 1021.8 eV which can be assigned to Zn 2p_{1/2} and Zn 2p_{3/2} core levels indicating +2 oxidation states on surface Zn ions [5, 11].

3. Characterization of ZnO- and ZnO@ZIF-8-based sensor material by simultaneous thermal analysis

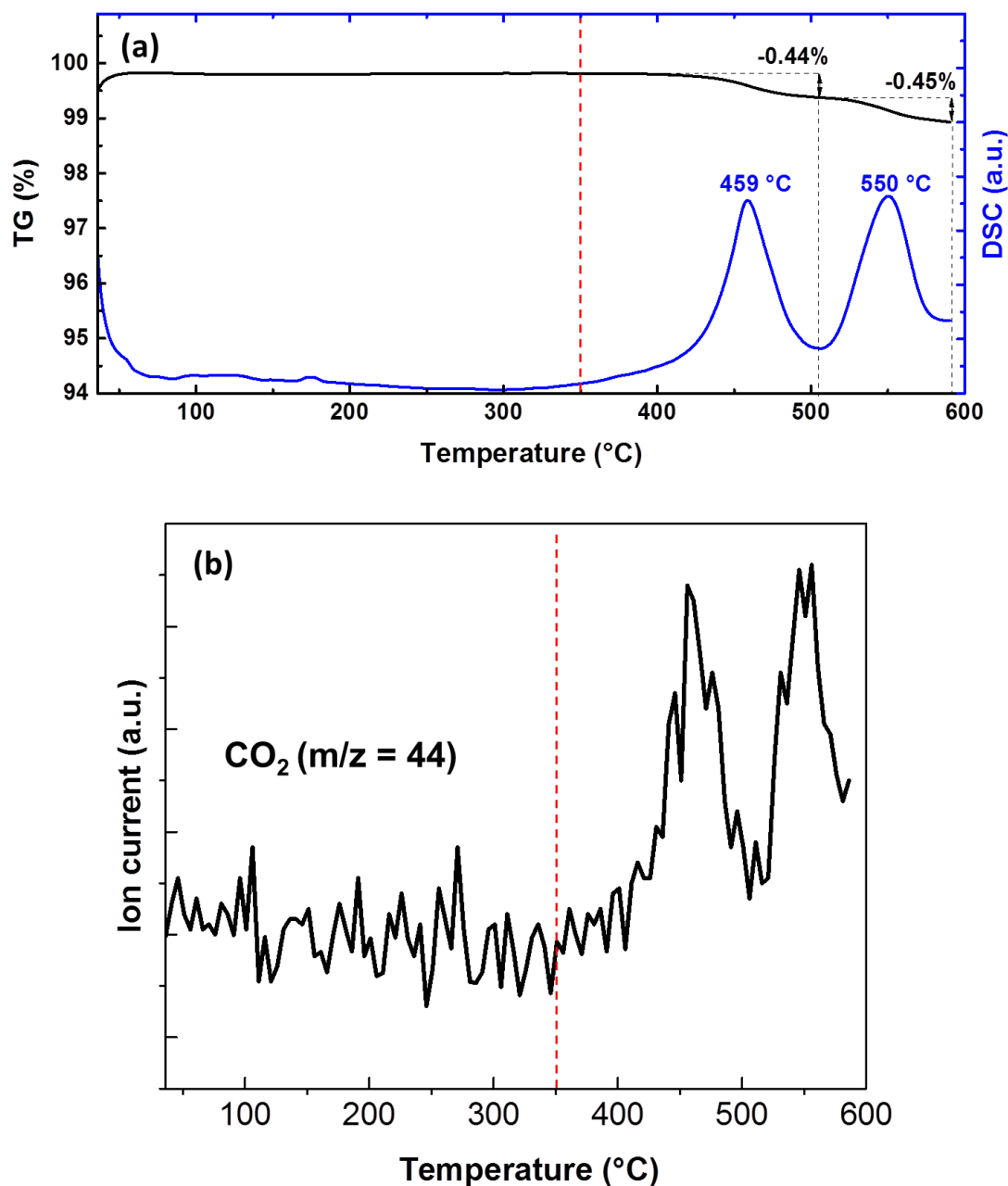


Figure S3: (a) STA analysis (TG = black curve; DSC = blue curve) of ZIF-8 membrane grown on a α -Al₂O₃ membrane. The red dashed line marks the operation temperature of the sensor at 350 °C. (b) MS curve of evolved CO₂ (m/z = 44).

The thermal stability of a ZIF-8 membrane grown on a α -Al₂O₃ membrane was investigated with simultaneous thermal analysis (STA). STA measurements were performed on a STA 449 C Jupiter (Netzsch-Gerätebau GmbH, Selb, Germany) equipped with a thermogravimetry/differential scanning calorimetry (TG/DSC) sample holder. The STA is connected to a quadrupole mass spectrometer (MS) 403 C Aëolos (InProcess Instruments

(IPI)/NETZSCH-Gerätebau GmbH, Selb, Germany) by a heated quartz glass capillary ($T = 230^{\circ}\text{C}$). Samples were heated at 10 K/min from 35 to 590°C in streaming dry air ($79\text{ mass-}\% \text{ N}_2 / 21\text{ mass-}\% \text{ O}_2$; SynA; 50 mL min^{-1} and $20\text{ mL min}^{-1} \text{ N}_2$). Aluminum crucibles (diameter 5 mm and height 3 mm) with a punched lid were filled with approximately 30 mg of material. An empty Aluminum crucible with lid served as inert reference sample.

The DSC showed two exothermal peaks at 459°C and 550°C (Fig. S3a). Both are associated with a mass loss in the TG curve (Fig. S3a) and with the release of CO_2 ($m/z = 44$; Fig. S3b) and H_2O (data not shown). The mass loss was 0.44% and 0.45% in range between 350°C and 590°C . The mass loss and the release of CO_2 and H_2O can be attributed to the decomposition of the ZIF-8 membrane. The low absolute mass loss of 0.44% and 0.45% is due to the small amount of ZIF-8 MOF material compared to the overall mass of the sensor chip. The operation temperature of the sensor at 350°C is far below the critical degradation temperature (459°C) of ZIF-8 (red dashed line in Fig. S3a and S3b).

4. Grand Canonical Monte Carlo (GCMC) method for calculating adsorption isotherms

To mimic the experimental composition of the mixtures, the total pressure of the propene/air and ethene/air gas mixtures were set to 1 bar. The mole fractions of propene and ethene were set to 5% and the oxygen mole fraction to 21%, according to the natural O₂ mole fraction in air. The mole fraction of water varied according to the rH conditions considered in the experiments, that is, 25%, 50% and 75%. The remainder of the mixture was set to be N₂, to create a mixture with a total pressure of 1 bar. Simulations for adsorption on the surface of ZnO were conducted at a sensor operating temperature of 350 °C and the amount of the adsorbed gas was determined as volume per cm² ZnO at standard temperature and pressure (STP) conditions. For ZIF-8 simulations the temperature of the inlet gas (25 °C) was assumed, since the thermal conductivity of MOF materials is known to be very poor and the adsorbed amount of gas is given by the volume of the gas under STP conditions per cm³ of ZIF-8 [12].

Grand canonical Monte Carlo (GCMC) method was used to simulate the adsorption of the propene-air and ethene-air mixtures in ZIF-8 and on ZnO surface. To mimic the experimental composition of the mixtures, the molar fraction of propene and ethene was set at 5% and the oxygen molar fraction at 21%. Water mol fraction varied with %rH value and the balance was nitrogen. The total pressure of both gas mixtures was set to 1 bar. Simulations for adsorption on the surface of ZnO were conducted at the sensor operating temperature (350 °C); whereas, in ZIF-8 simulations were conducted at the temperature of the inlet gas (25 °C) since thermal conductivity of MOF materials are known to be very poor [12]. All simulations were carried out with the RASPA [13] molecular simulation software. The ZIF-8 atoms were kept fixed at their experimentally determined crystallographic positions [14] and the ZIF-8 unit cell was replicated by 2 x 2 x 2 for the GCMC simulations. For ZIF-8 atoms force field parameters were taken from the work of Krokidas et al. [15]. Similarly, ZnO atoms were kept fixed at their experimentally determined crystallographic positions [16] after creating a non-polar surface (1010) on a slab with dimensions 22 x 31 x 38 Å in the x, y and z directions, respectively (Fig. S2). In order to avoid the artificial electrostatic interactions between the two ZnO surfaces, a vacuum space which is equal to 3 times of the thickness of the ZnO slab was added along the x direction, that is, perpendicular to the surfaces. Force field parameters for the ZnO structure were taken from the work of Nawrocki et al. [17]. N₂, O₂, ethene and propene molecules were modelled with the TraPPE-UA (Transferable Potentials for Phase Equilibria – United Atom) [18] force field and the TIP4P [19] model was used for water. Periodic boundary conditions were applied in all three dimensions and the cut-off distance was set to 14 Å. Ewald summation was used to compute coulombic interactions and short range interactions were handled with the Lennard Jones potential while using the Lorentz-Berthelot mixing rule to determine interaction parameters between alike atoms. Each simulation was equilibrated for 1 million cycles followed by a 1 million cycle production run. One cycle is equal to N steps, where N is the number of molecules present in the system. Translation, rotation, insertion and deletion moves were sampled with equal probability for water, oxygen, nitrogen and ethene or propene molecules.

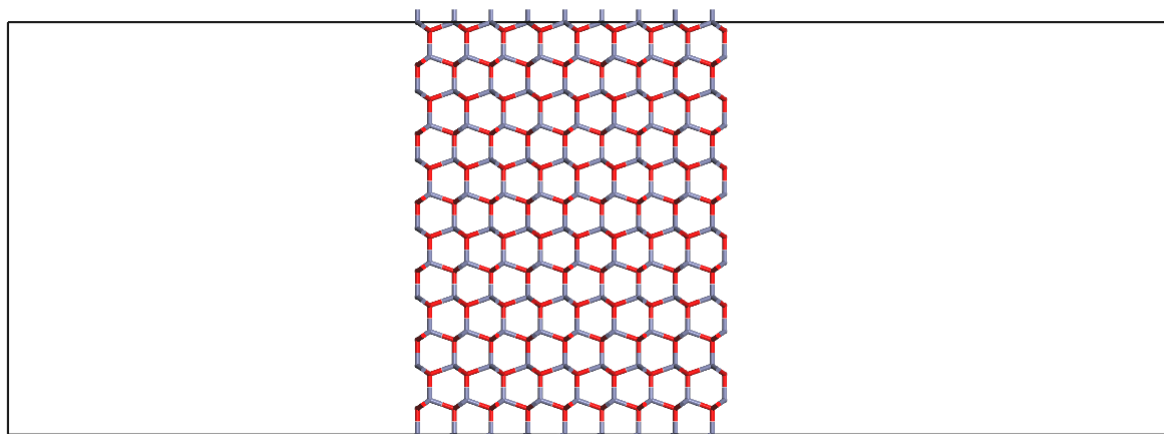


Figure S2. Zinc oxide (1010) slab. The total simulation box dimensions are 88 x 31 x 38 Å in the x, y and z directions, respectively.

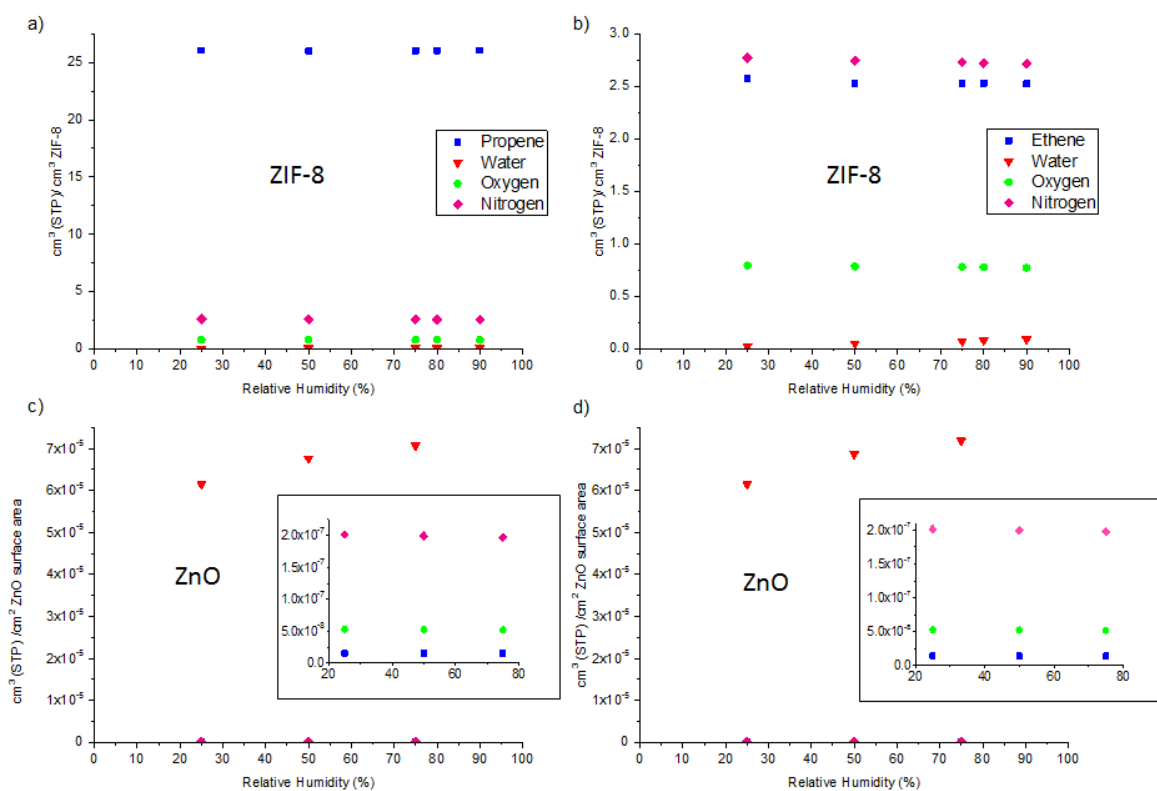


Figure S3: Simulated adsorption (i) of a propene/air (a) and an ethene/air (b) mixture in a ZIF-8 MOF and (ii) of a propene/air (c) and an ethene/air (d) mixture on a ZnO surface as function of rH. Due to the low adsorption of nitrogen, oxygen and target gas in the case of ZnO, the corresponding data are given in an expanded scale (inset of images (c) and (d)). Simulations in ZIF-8 were conducted at the gas temperature (25 °C) whereas for ZnO the sensor operating temperature (350°C) was taken into account.

References

- [1] M. Drobek, J.-H. Kim, M. Bechelany, C. Vallicari, A. Julbe, S. S. Kim, MOF-Based Membrane Encapsulated ZnO Nanowires for Enhanced Gas Sensor Selectivity, *ACS Appl. Mater. Interfaces* (2016) 8323-8328. <https://doi.org/10.1021/acsami.5b12062>.
- [2] W.-T. Koo, S.-J. Choi, J.-S. Jang, I.-D. Kim, Metal-Organic Framework Templated Synthesis of Ultrasmall Catalyst Loaded ZnO/ZnCo₂O₄ Hollow Spheres for Enhanced Gas Sensing Properties, *Sci.Rep. UK* (2017) 45074. <https://doi.org/10.1038/srep45074>.
- [3] N. Gogurla, A. K. Sinha, S. Santra, S. Manna, S. K. Ray, Multifunctional Au-ZnO Plasmonic Nanostructures for Enhanced UV Photodetector and Room Temperature NO Sensing Devices, *Sci. Rep. UK* (2014) 6483. <https://doi.org/10.1038/srep06483>.
- [4] Y. Pan, W. Liu, Y. Zhao, C. Wang, Z. Lai, Improved ZIF-8 membrane: Effect of activation procedure and determination of diffusivities of light hydrocarbons, *J. Membrane Sci.* (2015) 88-96. <https://doi.org/10.1016/j.memsci.2015.06.019>.
- [5] X. Hu, X. Yan, M. Zhou, S. Komarneni, One-step synthesis of nanostructured mesoporous ZIF-8/silica composites, *One-step synthesis of nanostructured mesoporous ZIF-8/silica composites* (2016) 311-316. <https://doi.org/10.1016/j.micromeso.2015.06.046>.
- [6] J. Liu, B. Lukose, O. Shekhah, H. K. Arslan, P. Weidler, H. Gliemann, S. Braese, S. Grosjean, A. Godt, X. Feng, K. Muellen, I.-B. Magdau, T. Heine, C. Woell, A novel series of isorecticular metal organic frameworks: realizing metastable structures by liquid phase epitaxy, *A novel series of isorecticular metal organic frameworks: realizing metastable structures by liquid phase epitaxy* (2012). 921
10.1038/srep00921.
- [7] F. Tian, A. M. Cerro, A. M. Mosier, H. K. Wayment-Steele, R. S. Shine, A. Park, E. R. Webster, L. E. Johnson, M. S. Johal, L. Benz, Surface and Stability Characterization of a Nanoporous ZIF-8 Thin Film, *J. Phys. Chem.* (2014) 14449-14456. 10.1021/jp5041053.
- [8] S. Luanwuthi, A. Kittayavathananon, P. Srimuk, M. Sawangphruk, In situ synthesis of permselective zeolitic imidazolate framework-8/graphene oxide composites: rotating disk electrode and Langmuir adsorption isotherm, *In situ synthesis of permselective zeolitic imidazolate framework-8/graphene oxide composites: rotating disk electrode and Langmuir adsorption isotherm* (2015) 46617-46623. 10.1039/c5ra05950j.
- [9] M. Chin, C. Cisneros, Stephanie M. Araiza, K. M. Vargas, K. M. Ishihara, F. Tian, Rhodamine B degradation by nanosized zeolitic imidazolate framework-8 (ZIF-8), *Rhodamine B degradation by nanosized zeolitic imidazolate framework-8 (ZIF-8)* (2018) 26987-26997. 10.1039/c8ra03459a.
- [10] S. Liu, Z. Xiang, Z. Hu, X. Zheng, D. Cao, Zeolitic imidazolate framework-8 as a luminescent material for the sensing of metal ions and small molecules, *Zeolitic imidazolate framework-8 as a luminescent material for the sensing of metal ions and small molecules* (2011) 6649-6653. 10.1039/c1jm10166h.
- [11] P.-Z. Li, K. Aranishi, Q. Xu, ZIF-8 immobilized nickel nanoparticles: highly effective catalysts for hydrogen generation from hydrolysis of ammonia borane, *ZIF-8 immobilized nickel nanoparticles: highly effective catalysts for hydrogen generation from hydrolysis of ammonia borane* (2012) 3173-3175. 10.1039/c2cc17302f.
- [12] B. Mu, K. S. Walton, Thermal Analysis and Heat Capacity Study of Metal–Organic Frameworks, *J. Phys. Chem. C* (2011) 22748-22754. <https://doi.org/10.1021/jp205538a>.
- [13] D. Dubbeldam, S. Calero, D. E. Ellis, R. Q. Snurr, RASPA: molecular simulation software for adsorption and diffusion in flexible nanoporous materials, *Mol. Simulat.* (2016) 81-101. <https://doi.org/10.1080/08927022.2015.1010082>.
- [14] K. S. Park, Z. Ni, A. P. Côté, J. Y. Choi, R. Huang, F. J. Uribe-Romo, H. K. Chae, M. O’Keeffe, O. M. Yaghi, Exceptional chemical and thermal stability of zeolitic imidazolate frameworks, *P. Natl. Acad. Sci. USA* (2006) 10186. <https://doi.org/10.1073/pnas.0602439103>.

- [15] P. Krokidas, M. Castier, S. Moncho, E. Brothers, I. G. Economou, Molecular Simulation Studies of the Diffusion of Methane, Ethane, Propane, and Propylene in ZIF-8, *J. Phys. Chem. C* (2015) 27028-27037. <https://doi.org/10.1021/acs.jpcc.5b08554>.
- [16] C. Wöll, The chemistry and physics of zinc oxide surfaces, *Prog. Surf. Sci.* (2007) 55-120. <https://doi.org/10.1016/j.progsurf.2006.12.002>.
- [17] G. Nawrocki, M. Cieplak, Amino acids and proteins at ZnO-water interfaces in molecular dynamics simulations, *Phys. Chem. Chem. Phys.* (2013) 13628-13636. <https://doi.org/10.1039/C3CP52198B>.
- [18] K. A. Maerzke, N. E. Schultz, R. B. Ross, J. I. Siepmann, TraPPE-UA Force Field for Acrylates and Monte Carlo Simulations for Their Mixtures with Alkanes and Alcohols, *J. Phys. Chem. B* (2009) 6415-6425. <https://doi.org/10.1021/jp810558v>.
- [19] W. L. Jorgensen, J. Chandrasekhar, J. D. Madura, R. W. Impey, M. L. Klein, Comparison of simple potential functions for simulating liquid water, *J. Chem. Phys.* (1983) 926-935. <https://doi.org/10.1063/1.445869>.